NASA TECHNICAL NOTE

NASA TN D-7604

NASA TN D-7604

THE STRESS CORROSION SUSCEPTIBILITY OF SEVERAL ALLOYS IN HYDRAZINE FUELS

by William P. Gilbreath and Michael J. Adamson

Ames Research Center
Moffett Field, Calif. 94035

NATIONAL AERONAUTICS AND SPACE ADMINISTRATION • WASHINGTON, D. C. • FEBRUARY 1974

1. Report No. D- 7604	2. Government Accession No.	3. Recipient's Catalog No.

4. Title and Subtitle	5. Report Date
THE STRESS CORROSION SUSCEPTIBILITY OF SEVERAL ALLOYS IN HYDRAZINE FUELS	February 1974
	6. Performing Organization Code
7. Author(s)	8. Performing Organization Report No.
William P. Gilbreath and Michael J. Adamson	A-5225
	10. Work Unit No.
9. Performing Organization Name and Address	501-21-21-05-00-21
NASA Ames Research Center Moffett Field, Calif., 94035	11. Contract or Grant No.
	13. Type of Report and Period Covered
12. Sponsoring Agency Name and Address	Technical Note
National Aeronautics and Space Administration Washington, D. C., 20546	14. Sponsoring Agency Code

15. Supplementary Notes

16. Abstract

The stress corrosion susceptibility of five alloys exposed to hydrazine and other related fuel environments is discussed on the basis of results from tests of crack growth in wedge opening loaded fracture specimens. It is shown that the alloys tested can be classified in order of decreasing susceptibility as follows: 4130 steel, 410 stainless steel, Inconel 718, Ti-6Al-4V (STA) and 6061-T6 Al; where the 4130 alloy shows a threshold stress intensity (K_{Iscc}) for flaw growth in hydrazine equal to about 20 percent of its fracture toughness (K_{Ic}) and the aluminum alloy shows no susceptibility. The specific fuels tested, listed in order of decreasing propensity to promote stress corrosion cracking, are: hydrazine, Aerozine 50, monomethylhydrazine, and unsymmetrical dimethylhydrazine (UDMH). Variation of a number of test parameters (load, load history, and impurity level) is shown to affect primarily the length of the incubation period before cracking initiates. Crack growth susceptibility is shown to be closely related to the contamination levels of water and carbon dioxide in the fuels and to the hydrogen ion concentration. Barium oxide additions to the fuels act to eliminate crack growth for test periods exceeding 4000 hours.

17. Key Words (Suggested by Author(s))	18. Distribution Statement
Stress corrosion cracking Propellants Hydrazine	Unlimited – Unclassified Cat.17

19. Security Classif. (of this report)	20. Security Classif. (of this page)	21. No. of Pages	22. Price*
Unclassified	Unclassified	19	$2.75

*For sale by the National Technical Information Service, Springfield, Virginia 22151

THE STRESS CORROSION SUSCEPTIBILITY OF SEVERAL ALLOYS IN HYDRAZINE FUELS

William P. Gilbreath and Michael J. Adamson

Ames Research Center

SUMMARY

The stress corrosion susceptibility of five alloys exposed to hydrazine and other related fuel environments is discussed on the basis of results from tests of crack growth in wedge opening loaded fracture specimens. It is shown that the alloys tested can be classified in order of decreasing susceptibility as follows: 4130 steel, 410 stainless steel, Inconel 718, Ti-6Al-4V (STA) and 6061-T6 Al; where the 4130 alloy shows a threshold stress intensity (K_{Iscc}) for flaw growth in hydrazine equal to about 20 percent of its fracture toughness (K_{Ic}) and the aluminum alloy shows no susceptibility. The specific fuels tested, listed in order of decreasing propensity to promote stress corrosion cracking, are: hydrazine, Aerozine 50, monomethylhydrazine, and unsymmetrical dimethylhydrazine (UDMH). Variation of a number of test parameters (load, load history, and impurity level) is shown to affect primarily the length of the incubation period before cracking initiates. Crack growth susceptibility is shown to be closely related to the contamination levels of water and carbon dioxide in the fuels and to the hydrogen ion concentration. Barium oxide additions to the fuels act to eliminate crack growth for test periods exceeding 4000 hours.

INTRODUCTION

During the past twenty years there have been a number of investigations of the static compatibility of various materials with rocket fuels and oxidizers. These studies have resulted in rather extensive compilations (refs. 1-5) of data concerning the compatibility of such fuels as hydrazine, pentaborane, JP-4, and hydrogen and of such oxidizers as nitrogen tetroxide, chlorine trifluoride, and oxygen with metal, ceramic, and elastomeric materials. The examinations have generally been cursory, except for those environment/material couples intended for actual application; because these at least attempt to simulate the time, temperature and static portions of the service profile. The general success of these test procedures has been borne out by the impressive number of successful missions. However, as systems expand in size and complexity, as more exotic materials (both propellants and components) are put into use, and as multicycle and long term usage become necessary, the need will increase for more exact simulation in compatibility testing, which will similarly increase in difficulty.

With the wide use of the hydrazine family of fuels, much test time has been devoted to static compatibility in which the basic concern has been the stability of the fuel in a given container material as a function of time at ambient temperatures. Additionally, some work has centered on the influence of specific impurities on the fuel stability (refs. 6-8). The possible detrimental effect

of the fuel on the component, if studied at all, has usually been of a secondary concern and has been considered from the standpoint of material loss and susceptibility to corrosion.

There has been very little done in the way of systematic examination of the possible effect that hydrazine fuels might have on the fracture behavior of various metal components in plumbing, tankage, and storage applications. Apparently, the work in this area has been limited to two studies involved with solving applied materials problems for specific missions. These studies indicate that under certain conditions hydrazine fuels can cause a reduction in the resistance to flaw growth in the two metals examined. Aerozine 50 [a 1:1 mixture by weight of hydrazine and unsymmetrical dimethylhydrazine (UDMH)] was found (ref. 9) to reduce the stress intensity necessary for growth in Ti-6Al-4V (solution treated and aged) to about 75 percent of fracture toughness. In contrast to these results, however, other workers observed no stress corrosion for the same system (ref. 10). More recently, 410 stainless steel, used as a tankage material in the Delta 89 vehicle, showed stress corrosion susceptibility with Aerozine 50 propellant (ref. 11). Experiments indicated that carbazic acid (H_2N_2 HCOOH, an impurity formed in hydrazine from carbon dioxide absorption) was one of the agents responsible for the cracking susceptibility. The magnitude of the apparent strength loss in the 410 alloy was not determined in these experiments. Conversely, Raymond and Usell (ref. 12) found no apparent stress corrosion in UDMH for several high toughness steels -- T-1, HY-140, HP-9-4-20, and 18Ni-(200) maraging steel -- that do stress corrode in such environments as seawater. Since stress corrosion does occur in a number of alloys in a variety of environments (ref. 13) and has been identified in the two instances cited with Aerozine 50, it is important that the parameters which influence stress corrosion cracking of metals in hydrazine propellants be investigated in order to provide logical design and material selection guidelines for components used in hydrazine service.

AISI 4130 steel, a high strength, low alloy material, was selected for detailed examination in this program. This steel is known (ref. 13) to be highly susceptible to stress corrosion cracking in a number of environments, and thus it was anticipated that this alloy would provide a good model for delineating various parameters (e.g., exposure period, stress level, or fuel constitution) which might be causative factors in the expected stress corrosion with hydrazine fuels. Although not generally used in hydrazine service, 4130 steel has been found (refs. 2, 5) to be compatible, based on static corrosion testing, with monomethylhydrazine (MMH), Aerozine 50, and UDMH. (While no specific reference is found for its compatibility with hydrazine, its usage, particularly at elevated temperature, should probably be proscribed because of its tendency to rust.) Additionally, several other alloys, 410 stainless steel, Ti-6Al-4V, 6061-T6 Al, and Inconel 718 have been examined in the present study for stress corrosion susceptibility. These alloys find major application for service with hydrazine and related fuels.

EXPERIMENTAL PROCEDURE

The stress corrosion experiments consisted of observing the tendency for flaw growth in wedge opening loaded (*WOL*) specimens of the various alloys when submerged in the fuels of interest. The specimens were heat treated, cleaned, fatigued to introduce a small flaw at the notch tip and loaded (either while in the fuel or in air).

The specimen configuration used in this study is shown in figure 1. All materials used were 0.32 cm thick. This thickness is too small to satisfy the ASTM thickness criterion (refs. 14, 15) for

valid plane-strain fracture toughness data (K_{IC}) for all of the alloys examined, with the possible exception of the 4130 steel. Nevertheless, threshold stress intensity values (K_{ISCC}) for the materials in the corroding environments could be measured and used to determine the stress corrosion susceptibility to be expected in the test medium. Nonstandard critical stress intensities for unstable crack growth are reported as K_Q. The specimen dimensions (other than thickness) conform closely to those of the ASTM compact tension (*CT*) specimen (ref. 15). However, the initial crack length to depth ratio was minimized to increase the growth length available for the flaw and thus increase the information that might be generated from a single specimen. The specimen was designed so it could be loaded by screwing a pipe-tapered plug (hardened tool steel) into the hole shown in figure 1.

After machining to size (fig. 1), the materials were heat-treated as follows: 4130 (1% Cr, 0.2% Mo, 0.3% max. C) was austenized at 1200° K, oil quenched and tempered at 525° K to a hardness of R_C 47. 410 stainless steel (12% Cr, 1% Mn, 0.8% Si, 0.15% max. C) was process annealed at 1050° K, heated to 1300° K, air quenched and tempered at 600° K to R_C 43. Inconel 718 (52.5% Ni, 18% Fe, 5.2% Cb, 3% Mo, 0.8% Ti, 0.6% Al, 0.2% Mn, 0.1% Cu) was solution treated for 1 hour at 1300° K, air cooled, aged for 8 hours at 1100° K, furnace cooled to 925° K and held for 16 hours, then air cooled to produce a R_C 45. Ti-6Al-4V was examined in both the mill annealed and hardened condition; for the latter, the alloy was held at 1250° K for 1-1/2 hours, water quenched, aged at 900° K and 825° K for 8 hours each, and air cooled to give R_C 38. The 6061-T6 Al was used as received (R_{30T}, 60). Following heat treatment, all materials were sand blasted and washed in distilled water and isopropanol. Additionally, the titanium material was cleaned in a HNO_3/HF solution to remove the surface scale formed during heat treatment. After cleaning and oven drying, the specimens are protected against further contamination by storage in a desiccator and by handling only with gloves.

Following cleaning, the specimens were fatigued in order to produce a fatigue crack at the notch tip. (In all cases the specimens were cycled in tension-tension fatigue to produce a crack extension 2 to 5 mm in length in 50,000 cycles.) The initial crack length (a_O) for the stress corrosion test was determined as the distance from the load line center to the fatigue crack tip on each side of the specimen.

For most experiments, the specimens were loaded while immersed in the fuel. The fuel level was adjusted to be above the crack tip but below the loading plug in order to minimize the possibility of galvanic or dissimilar metal effects. The specimens were placed in a specially constructed slotted polyethylene container and gripped by means of the 0.635 cm-diam holes which facilitated the loading. To minimize contamination of the fuel, the whole loading operation was performed in a dry nitrogen back-filled glove box. The specimens were loaded to a crack opening displacement corresponding to some stress-intensity level, K, below that required to propogate the crack in air, K_Q. As shown in appendix A, a knowledge of the crack length and displacement at the crack mouth opening (a constant during each experiment) allows one to calculate the stress intensity (K) at the crack-tip. This displacement value was measured, with a clip-on style crack opening gage positioned between the knife edges of the specimen while it was loaded with the pipe plug. In those instances where stress corrosion occurs, this stress-intensity resulting from the initial loading is greater than can be sustained when the specimen is in contact with the fuel. In these cases, the initial flaw will grow in length, lowering the stress-intensity until a final stress-intensity, K_{ISCC} (the threshold value for the particular specimen material/fuel combination) is reached and the crack arrests.

Following loading, the containers were covered, placed in desiccators, and stored in a glove box. Fuel aliquots were removed at intervals to analyze for possible pick-up of atmospheric contaminants. The specimens were examined at various elapsed times, depending on the rate of crack growth. Estimates of the crack length during testing were made as a function of exposure time to the fuel by noting apparent crack position in relation to a series of scribe marks on the specimen. A final, more reliable, measurement of crack length was made after termination of the test. Additionally, in some cases, the specimen was fractured completely following the stress corrosion test so that an accurate final crack length determination could be made.

The crack growth that occurs in the fuel was reported as a function of time. Parameters investigated were alloy history, initial stress-intensity, and fuel chemistry (i.e., purity and the effect of purposely added impurities). Figure 2 is a photograph of a specimen following immersion in fuel while under load. The loading plug is shown, and the scribe lines are visible. Crack growth, which has proceeded nearly to the bottom of the specimen, is clearly seen. Corrosion effects of the fuel, readily apparent with some couples, are barely discernible on this specimen.

Analyses of the fuels used in this study are tabulated in table 1. Water, ammonia, and carbon dioxide were determined by gas chromatography. Good separation was achieved using a Poropak T support for Carbowax 400 in a 0.6 cm-diam stainless steel column 3.1 m in length at 395° K. Aniline was determined spectrophotometrically by measuring the absorbance at 285 nm.

TABLE 1.– FUEL ANALYSIS[a,b]

Impurity	Hydrazine			Monomethyl hydrazine	Unsymmetrical dimethyl hydrazine
	MCB-97%	Propellant grade	Martin-Marietta refined	Aldrich-98%	Aldrich-99%
Water	0.90%	0.65%	0.37%	0.67%	0.23%
Aniline	.89	.22	<.001	<.001	<.001
Ammonia	.38	.35	.26	.093	.05
Carbon dioxide	.028	.018	.009	<.01	<.01
Iron	.7ppm	1.1 ppm	2.9 ppm	.5 ppm	.5 ppm
Copper	<.1	<.1	<.1	<.1	<.1
Nickel	<.2	<.4	.2	.1	.1

[a]The Aerozine 50 used in the present study was prepared as needed by mixing equal weights of the propellant grade hydrazine with the unsymmetrical-dimethyl hydrazine. Thus, the impurity composition in this fuel should reflect the blending of the two propellants.

[b]Major impurities on percent by weight basis and dissolved metals in parts-per-million by weight.

The dissolved content of three metal impurities (those usually reported (refs. 8, 16) to be the most prevalent in hydrazine fuels) was determined by atomic absorption spectroscopy. The Martin-Marietta hydrazine and the propellant grade material (from the Jet Propulsion Laboratory) were higher in metal ions than the other fuels, presumably because they were received and stored in stainless steel containers. (The other fuels were contained in glass vessels.)

RESULTS AND DISCUSSION

The curves plotted in figures 3 through 8 are representative of the results generated in the present study, and from these, the effect of an immersion period in a particular fuel on the stress corrosion susceptibility of a given alloy as a function of a number of parameters may be assessed. The data from which these plots and other results indicated in the text were derived are presented in appendix B. Figure 3 is typical of these plots and shows the influence that initial stress intensity was found to have on 4130 steel in propellant grade hydrazine. Specimens were loaded to initial stress intensities below that required for crack extension in air (labeled K_Q, about 75 MN m^{-2} $m^{1/2}$). The initial load was found to affect, primarily, the incubation period duration; larger initial stress intensities were found to shorten this stable period before crack growth commences. Initial load was found in these and other tests (appendix B) to have no effect on the threshold stress intensity value (K_{ISCC}) of about 10 MN m^{-2} $m^{1/2}$. Experiments in which the bolt load was increased from the initial value following a given immersion period with no crack growth at the initial (lower) value (dashed line, fig. 3) resulted in growth behavior concordant with that of tests run solely at the higher load. That is, if the submersion period at the lower load was longer than the required incubation period at the high stress intensity, crack growth commenced immediately on increasing the load to the higher value.

This would indicate that the mechanism of the initial phase of attack includes a step that is purely corrosive in nature and probably stress independent. The *duration* of this initial phase does, however, depend on load. After a certain degree of corrosion or material damage occurs, the applied stress will be sufficient to initiate cracking while at larger applied stresses, less corrosion is necessary for crack growth to initiate, and thus there is a decrease in incubation time.

Another example of stress dependency of the incubation period and further evidence of the role of corrosion is illustrated in figure 4. In these experiments, the behavior of 4130 steel loaded while submerged was compared with specimens in which the initial stress intensity was applied in air and exposed for several hours to air prior to immersion (preloaded). As shown, preloading in air caused a large increase in the incubation period but did not affect K_{ISCC} for specimens in hydrazine. Apparently, the air exposure caused a semi-protective film to form which necessitates much longer exposure to the corrosive medium before sufficient bond weakening occurs to allow crack extension. However, at a greater initial K, 55 MN m^{-2} $m^{1/2}$, where less corrosion would be necessary prior to crack growth, preloading had much less effect on the incubation period (appendix B, specimen F-18).

On the same figure, comparative results are presented for solution- and preloaded-specimens of 4130 in MMH. In this case, however, the divergent initial loads imposed on the specimens apparently mask the role of load history. In any event (as will also be shown by data presented later), the MMH appears to be much less corrosive than propellant grade hydrazine, and the incubation period is considerably longer.

Figure 5 compares the effect of four fuel environments on stress corrosion susceptibility in solution-loaded 4130 steel specimens. For exposures up to at least 2000 hours and even at high stresses, UDMH caused no crack extension, while MMH caused growth after 500 hours exposure and hydrazine after about 60 hours. This is the same ordering as usually given for the stabilities of these fuels toward various metals and catalysts (refs. 1,2). Aerozine-50 showed about the same

effect on 4130 as did the hydrazine. The relatively benign nature of UDMH would indicate that the active agent in A-50 is hydrazine. Further experiments (appendix B) with various molar mixtures of UDMH and hydrazine showed that the latter component caused crack growth at concentrations down to at least 10 percent. The data suggests that the threshold intensity for 4130 in MMH is about twice that in hydrazine, or about 25 MN $m^{-2}\,m^{1/2}$.

The comparative effect of propellant grade hydrazine on specimens of Inconel-718, 410 stainless steel, Ti-6Al-4V, 6061-T6 Al, and 4130 steel is shown in figure 6. The applied stress intensities were all roughly 80 percent of K_Q. Crack growth commenced in the Inconel specimens after about 100 hours and continued to 4000 hours, when the tests were terminated. The final stress intensity observed was 80 MN m^{-2} $m^{1/2}$. No information is found in the literature on the stress corrosion susceptibility of Inconel alloys exposed to hydrazine propellants. Similarly, the 410 alloy was characterized by an extended period of slow crack growth, although the incubation period was about four times as long as that observed for Inconel-718. For this alloy, K_{Iscc} was approximately 30 MN m^{-2} $m^{1/2}$. Investigators at McDonnell Douglas Aircraft showed that 410 stainless steel will undergo stress corrosion cracking in Aerozine 50 (ref. 11). Their work was not quantitative, however, and no determination of K_{Iscc} was made. The results for 4130 have been discussed. In comparison to the other materials shown in figure 6, it is much more susceptible to stress corrosion cracking in hydrazine.

No crack growth was noted for Ti-6Al-4V (for specimens in both the mill anneal and heat treated conditions). These results (fig. 6) do not agree with those reported by Tiffany and Masters (ref. 9), who found a K_{Iscc} of 42 MN m^{-2} $m^{1/2}$ with a value of 0.80 for K_{Iscc}/K_{Ic} for material of a similar heat treatment in Aerozine 50. Using specimens fabricated from Lunar Module propellant tank forgings of solution treated and aged material, Bixler (ref. 17) reported a K_{Iscc} of about 45 MN m^{-2} $m^{1/2}$ and a value of 0.75 for K_{Iscc}/K_{Ic}. Both of these investigators used a part-through surface-crack specimen configuration having a material thickness of 0.14 cm and 0.3 cm in the case of Tiffany and Masters (ref. 9) and 0.23 cm for Bixler (ref. 17). The reason for the disagreement between these referenced investigators and the present work is not entirely clear. Possibly, the explanation may lie in the different specimen configurations employed. The specimens of the thickness used in these studies do not provide comparable values among different specimen configurations and test techniques. The critical stress intensity values reported by these workers (refs. 9, 17) do not agree with values given elsewhere (refs. 18, 19). For solution treated and aged Ti-6Al-4V, Blackburn et al. (ref. 18) report, in a summary of stress corrosion cracking in titanium alloys, a K_Q of over 100 MN m^{-2} $m^{1/2}$ for specimens of 0.14 cm thickness and 50 MN m^{-2} $m^{1/2}$ for 1.2 cm material. Additionally, Blackburn (ref. 18) gives a K_{Iscc}/K_Q of 0.7 and 0.55, respectively, for the two thicknesses in a 3.5 percent sodium chloride solution. Nelson et al. (ref. 19) in a comprehensive study of stress corrosion cracking in Ti-6Al-4V of various heat treatments, reported a K_Q of 132 MN m^{-2} $m^{1/2}$ and K_{Iscc}/K_Q of 0.86 for specimens of 0.3 cm thickness in the solution treated and aged condition on exposure to low pressure gaseous hydrogen. It is apparent that, regardless of the various K_Q values reported in the different studies, the K_{Iscc}/K_Q ratio was always close to 0.8 for thin specimens. For the heat treated specimens used in the present study, K_Q was found to vary from 100 to 110 MN m^{-2} $m^{1/2}$. Thus, since the applied intensities were all lower than 80 MN m^{-2} $m^{1/2}$ (appendix B), it is likely that the cracking threshold was not achieved. (In the present study, extreme galling between bolt and specimen prevented higher intensities from being applied.) Brownfield (ref. 10) found no stress corrosion cracking in edge-notched tensile specimens of Ti-6Al-4V in the solution treated and aged condition when submerged in Aerozine-50 for periods up to 71 days. The author gives no stress intensities for the material, but from the given applied load and specimen

configuration, one may calculate, using the equation of Bowie (ref. 20) an applied K of 35.6 MN m^{-2} $m^{1/2}$. This value is probably too low for crack growth to occur.

No evidence of crack extension was found in the 6061-T6 aluminum specimens, even at stress intensities close to K_Q (about 30 MN m^{-2} $m^{1/2}$). Muraca et al. (ref. 8) report that this particular alloy is compatible with hydrazine, at least under static test conditions, in that it does not cause enhanced decomposition of the fuel at 320° K for 4-year storage periods. Although aluminum alloys are fairly widely used with hydrazine fuels, apparently there are no published results on the stress corrosion susceptibility of these couples. Piper,[1] in an unpublished study, found no stress corrosion in 7079-T651 aluminum immersed for up to 1 month in hydrazine.

The effect of two common impurities, water and carbon dioxide, on stress corrosion cracking in hydrazine fuels was examined in detail. High purity hydrazine readily absorbs these impurities from the air, and, since water is also a product of the oxygen/hydrazine reaction, these contaminants are always present to an extent dictated by the care exercised to exclude atmospheric contact in both the manufacturing process and subsequent handling. Figure 7 shows that for the system 4130/hydrazine the presence of water acts to change the incubation period and thus, as discussed earlier, probably the corrosiveness of the fuel. K_{Iscc} was unaffected, but, perhaps, a slight crack-growth rate increase is caused by the presence of water. The curve for 0.9 percent water by weight is for the MCB fuel but also should represent the behavior of propellant grade fuel with 0.6 percent water, since the results are not sensitive to small changes in water content. Recently revised Mil-Specs (MIL-P-26536c) call for a maximum water content of 1 percent by weight in the propellant grade hydrazine. These same specifications limit carbon dioxide to 200 ppm (0.02 percent by weight).

The effect of hydrazine with a carbon dioxide impurity level of 200 ppm on the stress corrosion properties of 4130 is shown in figure 8. Also shown for comparison is the effect caused by 1 percent carbon dioxide and by BaO treated hydrazine. Although analysis techniques employed did not provide a reliable measurement of the free carbon dioxide in the fuel samples treated with barium oxide, the barium oxide treatment ties up the carbon dioxide as the insoluble carbonate; and other workers[2] estimate the free carbon dioxide concentration in such a system as under 20 ppm.[3] The concentration of carbon dioxide has a much greater effect on the stress corrosion susceptibility of 4130 steel (fig. 8) than did water contamination (fig. 7).[4] Again, however, the effect was primarily on the incubation period.

From these results it would appear that pure hydrazine (i.e., devoid of carbon dioxide contamination) would have no effect on 4130 steel from a stress corrosion standpoint. Immersion tests with this couple are still in progress. Other experiments (appendix B) using carbon dioxide contaminated and barium oxide treated hydrazine with 410 stainless alloy have yielded similar results. Further tests with the barium oxide treated hydrazine/4130 steel system have shown

[1] Piper, Don: Lockheed Missiles and Space Corp. Private communication.

[2] Vango, Sterne: Jet Propulsion Laboratories. Private communication.

[3] This appears to be an area of some controversy, as Axworthy et al. (ref. 6) state that the BaO treatment does not lower the CO_2 content below 200 ppmw. If this is correct, then the exact role of the BaO is difficult to comprehend. Axworthy does show that BaO treatment reduces the hydrazine decomposition rate by at least a factor of 10.

[4] In fact since the 0.9 percent water curve (fig. 7) and the 200 ppmw CO_2 curve (fig. 8) represent the normal, unadulterated fuel the former curve probably results, primarily from the effect of the CO_2 impurity. This supposition is given further support by considering the results derived from the BaO treated fuel (fig. 8), in which the CO_2 was tied up but the water content was probably not reduced (ref. 6).

(appendix B, specimen F-20) that if, after immersion for a period when no crack growth occurs, untreated hydrazine is substituted for the BaO treated fuel, crack growth will commence within a short period. This incubation time is less than would be expected if a specimen under similar load were immersed in only the untreated hydrazine. It appears that even the treated fuel has some corrosive effect on the alloy. However, when substitution of treated for the untreated fuel was made during crack growth, the crack was arrested at a stress intensity above the normally observed K_{Iscc} value.

A commonality exists between solutions of water and carbon dioxide in hydrazine in that both are sources of protons, viz:

$$H_2O + N_2H_4 = N_2H_5^+ + OH^- \quad (1)$$

and

$$CO_2 + N_2H_4 = H_2N_2HCOO^-H^+ \quad (2)$$

The latter product, carbazic acid, is probably more correctly characterized in excess hydrazine as the hydrazinium salt, $H_2N_2HCOO^-N_2H_5^+$. The hydrazinium ion, $N_2H_5^+$, in hydrazine is the analog in properties of the hydronium ion, H_3O^+, in water. Simplistically, a measure of the hydrazinium ion concentration may be calculated for systems containing the two impurities by using the equilibrium constant (ref. 23) for reaction (1), $K_{298} = 8.5\times10^{-7}$,[5] and assuming for reaction (2) that carbazic acid is a strong acid and the CO_2 reaction with N_2H_4 is complete. Thus, for small amounts of water, the hydrazinium ion will be proportional to the half-power of the water concentration and at a 1 percent impurity level would be 7×10^{-4} M. Assuming complete ionization, the hydrazinium ion concentration in reaction (2) is directly proportional to the carbon dioxide impurity level, which for the propellant grade hydrazine at 200 ppm would be equivalent to 4.5×10^{-3} M.

If the cause of stress corrosion cracking observed in the present study is hydrogen embrittlement, either by direct metal absorption of protons or by hydrogen formation at the metal surface following oxidation of the metal, the rate of crack growth or severity will be related to the hydrogen activity at the metal/solution interface. Using this argument, one can explain the relatively more active role that small amounts of carbon dioxide play compared to larger quantities of water impurities (figs. 7 and 8) in promoting stress corrosion cracking. Further, the reason for the effectiveness of a basic oxide addition (i.e., BaO) to hydrazine in eliminating or arresting crack growth is apparent. The BaO can neutralize the acid ion and precipitate the carbon dioxide as the carbonate, thus lowering the hydrogen activity.

CONCLUDING REMARKS

The primary objective of the study, to demonstrate the stress corrosion cracking tendencies of several important aerospace alloys in hydrazine family of fuels, was accomplished. Two alloys, widely used in propellant hardware, 410 stainless steel and Inconel-718, exhibited gross deterioration in their fracture behavior on immersion in hydrazine. Conversely, Ti-6Al-4V retained at least

[5] This is the equilibrium constant for dilute solutions of hydrazine. The constant, which would be more strictly applicable to this reaction, for dilute solutions of water in hydrazine, has apparently not been determined.

80 percent (the limit of the experiments) of its normal strength, and 6061-T6 aluminum evidenced no tendency toward stress corrosion cracking. Data derived from experiments with 4130 steel showed that variations in carbon dioxide and water impurity levels, initial stress intensity, fuel type, and stress history mainly affected the duration of the incubation period before crack growth occurs. The results prove the necessity of examining proposed fuel/metal systems for stress corrosion susceptibility in order to develop meaningful guidelines for both design and usage, which in turn are required to prevent the growth of undetected flaws and resultant system failure under stress.

Ames Research Center
National Aeronautics and Space Administration
Moffett Field, Calif., Nov. 12, 1973

APPENDIX A

BASIS FOR STRESS INTENSITY DETERMINATIONS

As noted in the text, the stress intensity for the specimen could be determined, either initially or following crack growth, by measuring the crack mouth opening displacement, V (a constant for a given experiment), and the instantaneous crack length, a. This was made possible by developing a calibration for the specimen response to load in the following manner: First, the compliance, C, was determined for specimens of the configuration shown in figure 1 by measuring V (using a clip-on style strain gage) for a given load as a function of crack length, a. The crack was simulated by slotting the specimen with a 0.05 cm thick saw blade. About 50 determinations were made on three specimens in this manner with "cracks" ranging in length from 1.5 to 4.7 cm. Next the data were fitted to a fourth degree exponential power function which was found to represent the data. The opening mode stress intensity factor, K, could then be determined from the relation:

$$K = \frac{V[(E/2B)(dC/da)]^{1/2}}{C} \tag{1}$$

where E is Young's modulus and B is the specimen thickness. (This equation may be derived from the K definition $(EG)^{1/2}$, where G is strain energy release rate.)

The experimentally determined relation is plotted in figure 9 in the form K/V vs. a/W, where W is the beam depth of the specimen (fig. 1, 5.08 cm). As a comparison, two other curves, purely analytical, are shown on the same figure. One was derived from the boundary collocation method described by Gross et al. (ref. 22) and the other, using the finite length beam with the elastic foundation model of Kanninen (ref. 23). In both cases, it was necessary to correct the load line displacements to crack mouth displacements needed in the present study – the parabolic approximation of Roberts (ref. 24) was used for this purpose. The three curves show fair agreement and the K values were found by using an average, weighted toward the experimentally determined data. Below $a/W = 0.3$ and above 0.9, the experimental curve represents an extrapolation of the compliance data, so more weight was attached to the analytical curves in these regions. As the a/W ratio approaches unity, the relations used to determine the curves are of doubtful validity. This is probably true beyond $a/W = 0.9$, and in several instances of severe stress corrosion susceptibility cracks went beyond this limit before arresting. The extreme case was specimen F-19 (appendix B) which reached $a/W = 0.95$; hence, the K_{final} value found for it, 6 MN m^{-2} $m^{1/2}$, is probably suspect.

APPENDIX B

DATA SUMMARY

The following tabulation summarizes the data derived from specimens of the various alloys examined for stress corrosion susceptibility under the conditions stated. Code: MCB, Matheson-Coleman-Bell 97 percent grade hydrazine; PG, propellant grade hydrazine obtained from JPL; MM, Martin-Marietta refined grade hydrazine; A-50, Aerozine 50; MMH, Aldrich 98 percent grade monomethyl hydrazine; UDMH, unsymmetricaldimethyl hydrazine; (P) refers to specimen preloaded in air before immersion in fuel; *, no crack growth noted under conditions of test; and †, test still in progress at immersion time noted.

Alloy	Specimen	Fuel	$K_{applied}$, MNm^{-2} $m^{1/2}$	Immersion period, hr	Incubation period, hr	K_{final}, MNm^{-2} $m^{1/2}$
6061-T6 aluminum	A-1	UDMH	21.8	125	*	21.7
	A-1a	UDMH	25.8	150	*	25.8
	A-1b	UDMH	30.7	72	*	30.7
	A-1c	A-50	30.7	168	*	30.7
	A-2	PG	27.5	864	*	27.5
	A-3	A-50/1% CO_2	21.5	440	*	21.5
	A-4	MCB/30% H_2O	18.0	74	*	18.0
	A-5	MCB/30% H_2O	24.0	100	*	24.0
Inconel-718	I-1(P)	A-50	119.7	3360†	900	87.7
	I-2	MCB	28.4	648	*	28.4
	I-2a(P)	MM	143.5	3550	80	130.0 (branched)
	I-3	PG	127.0	3130†	140	79.8
	I-4	MCB	65.7	900	*	65.7
	I-5(P)	MM	71.8	384	*	71.8
	I-5a(P)	MM/2% O_2	71.8	450	*	71.8
4130 steel	F-1	MCB	34.2	110†	60	17.0
	F-2	MM	46.8	120	50	7.9
	F-3	UDMH + 20% PG	43.2	210	75	13.0
	F-4	MCB + 5% H_2O	40.3	220	34	15.3
	F-5(P)	PG	25.3	600	290	12.8
	F-6	MMH	34.3	1280	*	34.3
	F-7	A-50	40.2	160	60	13.3
	F-8	PG + 6% H_2O	34.0	150	32	9.5
	F-9	PG + 30% H_2O	15.7	75	*	15.7
	F-9a	PG + 30% H_2O	23.0	100	48	11.9
	F-10	MCB	17.8	312	125	11.4
	F-11	PG + BaO	45.4	2260	*	45.4
	F-12(P)	A-50	29.1	408	*	29.1
	F-12a(P)	PG	29.1	180	*	29.1
	F-12b(P)	A-50 + 2% CO_2	29.1	504	20	14.5
	F-13	MCB + 30% H_2O	30.0	30	8	7.1
	F-14	UDMH	54.3	600	*	54.3
	F-14a	UDMH + 10% PG	45.8	280	88	14.8

Alloy	Specimen	Fuel	$K_{applied}$, MNm^{-2} $m^{1/2}$	Immersion period, hr	Incubation period, hr	K_{final}, MNm^{-2} $m^{1/2}$
4130 steel (concluded)	F-14b	UDMH	41.4	800	*	41.4
	F-15	PG	41.8	130	39	12.4
	F-16	MMH	44.5	2000†	670	37.5
	F-16a	PG + 1% CO_2	37.8	82	15	13.1
	F-17(P)	MMH	58.7	3800	500	22.8
	F-18(P)	PG	53.4	105	15	9.5
	F-19	MM + 5% H_2O	36.9	140	50	6.0
	F-20	PG + BaO	31.2	480	*	31.2
	F-20a	PG	31.2	48	16	20.1
	F-20b	PG + BaO	20.1	200	24 (arrested)	18.6
	F-21	PG	31.5	285	50	10.4
	F-22	UDMH	63.2	2000	*	63.2
410 stainless steel	N-1	MCB	31.5	200	*	31.5
	N-1a	MM	50.8			
	N-2	PG	50.0	245	*	50.0
	N-2a	PG/1% CO_2	44.5	220	24	30.2
	N-3a	PG/BaO	68.5	1400	*	68.5
	N-4	PG	61.7	640	*	61.7
	N-4a	PG/0.2% CO_2	61.7	168	20	31.1
	N-5	UDMH	67.4	3060†	*	67.4
	N-5a	A-50	57.5	1040	290	33.5
	N-6	MMH	47.1	3320	*	47.1
	N-7(P)	A-50	53.3	4600	*	53.3
	N-8	MM	20.2	460	*	20.2
	N-9	MCB	71.2	3140	380	39.8
	N-10	PG	61.5	420	*	61.5
	N-11(P)	PG	61.1	510	*	61.1
Ti-6Al-4V (mill anneal) ↓ (heat treated) ↓	T-1(P)	A-50	74.8	940	*	74.8
	T-2	MCB	42.4	900	*	42.4
	T-2a	MCB/1% CO_2	44.8	650	*	44.8
	T-3	MM	70.6	880	*	70.6
	T-4(P)	PG	50.7	1600	*	50.7
	T-6	PG	64.4	3250	*	64.4
	T-7(P)	PG	75.8	2920	*	75.8

REFERENCES

1. Uney, P. E.; and Fester, D. A.: Material Compatibility With Space Storable Propellant Design Guidebook. Rep. MCR-72-26, Martin-Marietta, 1972.

2. Anon.: Advanced Spacecraft Valve Technology Compilation, Vol. 1, Mechanical Controls. Rep. No. 12411-6012-R000, Thompson Ramo Woolridge (TRW), 1970.

3. Coulbert, C. D.; and Yankura, G.: Survey of Materials for Hydrazine Propulsion Systems in Multicycle Extended Life Applications. NASA TM 33-561, 1972.

4. Anon.: Liquid Rocket Tanks and Components. NASA Space Vehicle Design Criteria (Chemical Propulsion). NASA SP-8, 1971.

5. Boyd, W. K.; Berry, W. E.; and White, E. L.: Compatibility of Materials With Rocket Propellants and Oxidizers. DMIC Memorandum 2C1, Battelle-Columbus Laboratories, 1965.

6. Axworthy, A. E.; Cohz, S.; Sullivan, J. M.; and Welz, E.: Research on Hydrazine Decomposition. Rocketdyne Final Report AFRPL-TR-69-146, Calif., 1969.

7. Schmidt, E. W.: Contamination Effects in Hydrazine Engines. Rocket Research Corp., Engineering Study 72, Wash., 1972.

8. Muraca, R. F.; Crutchfield, C. A.; and Whittick, J. S.: The Results of Long-Term Storage Tests for Compatibilities of Spacecraft Materials With Hydrazine and Hydrazine Mixtures. SRI Rep. 951581-6, Palo Alto, Calif., 1967.

9. Tiffany, C. F.; and Masters, J. N.: Investigation of the Flaw Growth Characteristics of 6Al-4V Titanium Used in Apollo Spacecraft Pressure Vessels. NASA CR-65586, 1967.

10. Brownfield, C. W.: The Stress Corrosion of Titanium in Nitrogen Tetroxide, Methyl Alcohol and Other Fluids. Rep. 67-213A, Space Division, North American Rockwell, 1967.

11. Anon.: Delta Baseline Review. NASA-Goddard Space Flight Center, 1972, Sec. 6, pp. 1-2.

12. Raymond, L.; and Usell, R. J., Jr.: The Effect of N_2O_4 and UDMH on Subcritical Crack Growth in Various High-Toughness Low Strength Steels. TR-0059(6250-10)-8, Aerospace Corp., El Segundo, Calif., 1971.

13. Anon.: Damage Tolerant Design Handbook. MGIC-HB-01, Battelle-Columbus Laboratories, 1972.

14. Brown, W. F.; and Srawley, J. E.: Plane Strain Crack Toughness Testing of High Strength Metallic Materials. ASTM STP 410, American Society for Testing and Materials, Philadelphia, 1967.

15. Brown, W. F. (ed.): Review of Developments in Plane Strain Fracture Toughness Testing. ASTM STP 463, American Society for Testing and Materials, Philadelphia, 1970.

16. Salvinski, R. J.: Investigation of the Formation and Behavior of Clogging Material in Earth and Space Storable Propellants. Rep. 08113-6061-R000, TRW, Redondo Beach, Calif., 1968.

17. Bixler, W. D.: Fracture Characteristics of 6Al-4V Titanium Alloy Forgings Containing Alpha Stringer Microstructure. NASA CR-99512, 1969.

18. Blackburn, M. J.; Feeney, J. A.; and Beck, T. R.: Stress Corrosion Cracking of Titanium Alloys. Rep. D1-82-1054, The Boeing Co., Seattle, Wash., 1970.

19. Nelson, H. G.; Williams, D. P.; and Stein, J. E.: Environmental Hydrogen Embrittlement of an α-β Titanium Alloy; Effect of Microstructure. Met. Trans., vol. 3, Feb. 1972, pp. 469-475.

20. Bowie, O. L.: Rectangular Tensile Sheet With Symmetric Edge Cracks. Paper 64-APM-3, American Society of Mechanical Engineers, 1964.

21. Raphaelian, L. A.: Hydrazine and Its Derivatives in Applied Science and Technology. Vol. II. H. W. Wilson, 1969, p. 165.

22. Gross, B.; Roberts, E., Jr.; and Srawley, J. E.: Elastic Displacements for Various Edge-Cracked Plate Specimens. Intl. J. Fracture Mech., vol. 4, no. 3, Sept. 1966, pp. 267-276.

23. Kanninen, M. F.: An Augmented Double Cantilever Beam Model for Studying Crack Propagation and Arrest. Intl. J. Fracture Mech., vol. 9, no. 1, Mar. 1973, pp. 83-92.

24. Roberts, E., Jr.: Elastic Crack-Edge Displacements for the Compact Tension Specimens. Materials Research and Standards, MTRSA, vol. 9, no. 2, Feb. 1969, p. 27.

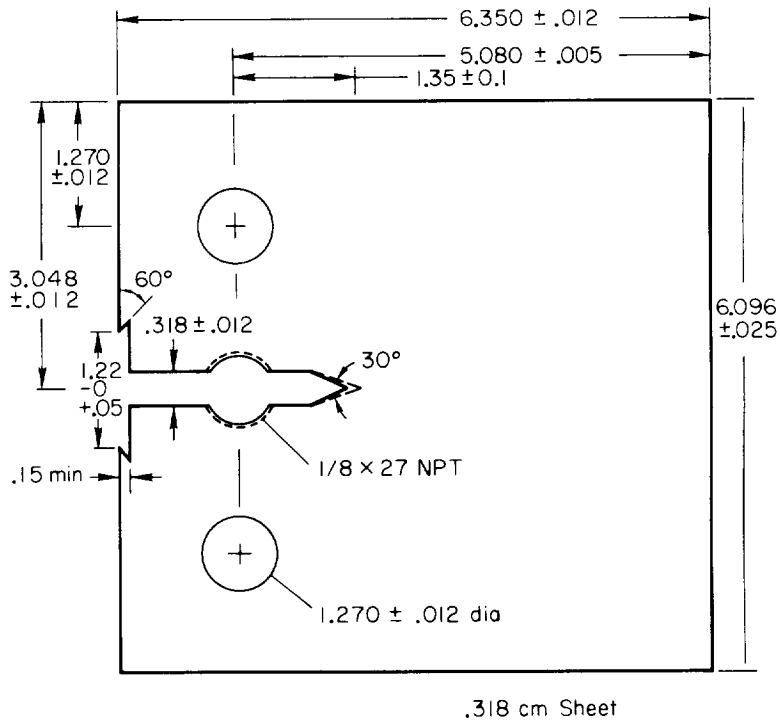

Figure 1.-- Specimen configuration for stress corrosion susceptibility study. Dimensions in cm, scale 2X.

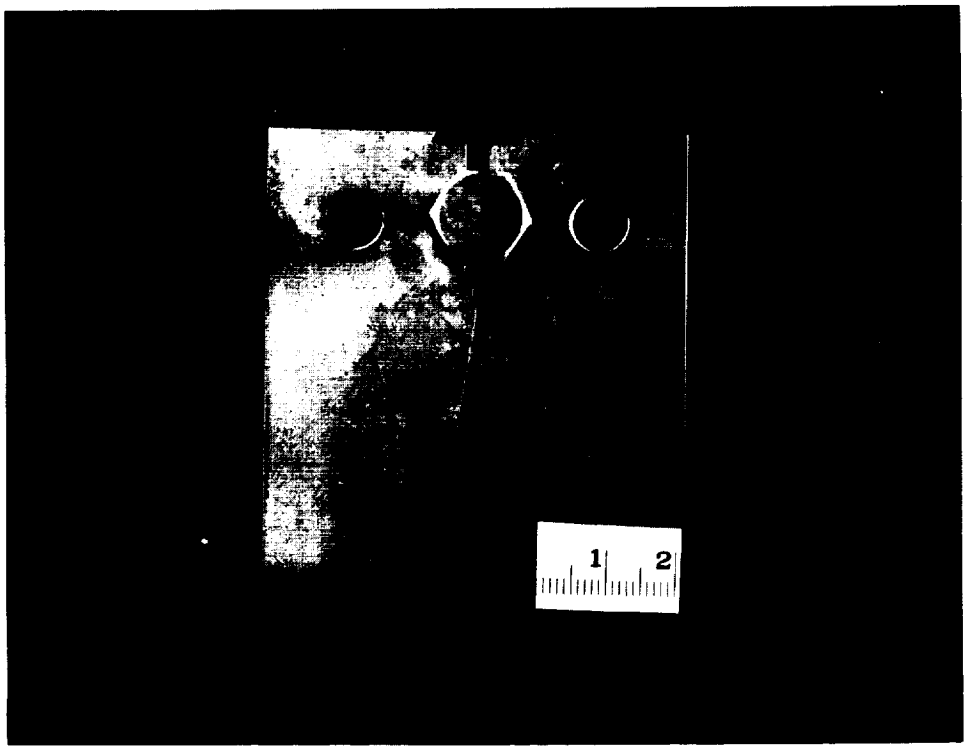

Figure 2.-- Photograph of specimen following stress corrosion testing; scale in cm.

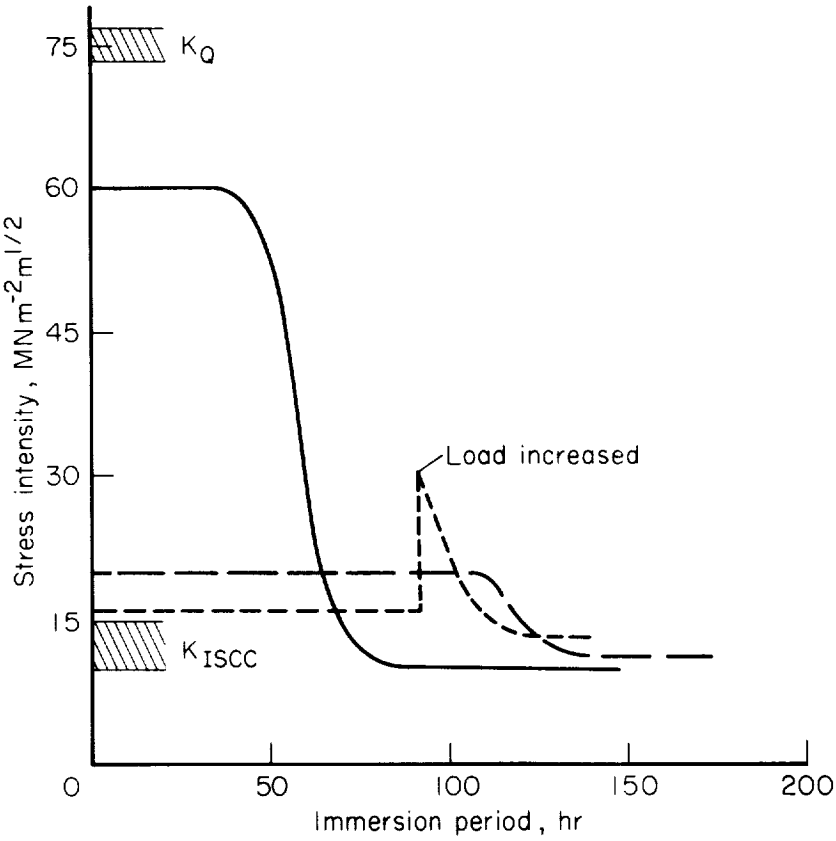

Figure 3.– The effect of stress level on the stress corrosion susceptibility of 4130 steel in hydrazine.

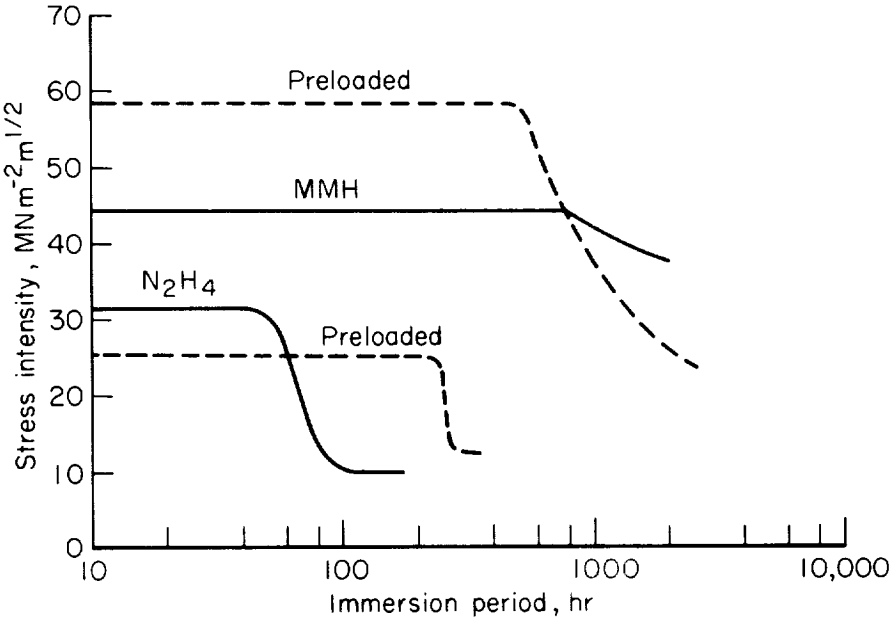

Figure 4.– The effect of load history on the stress corrosion susceptibility of 4130 steel in two fuels.

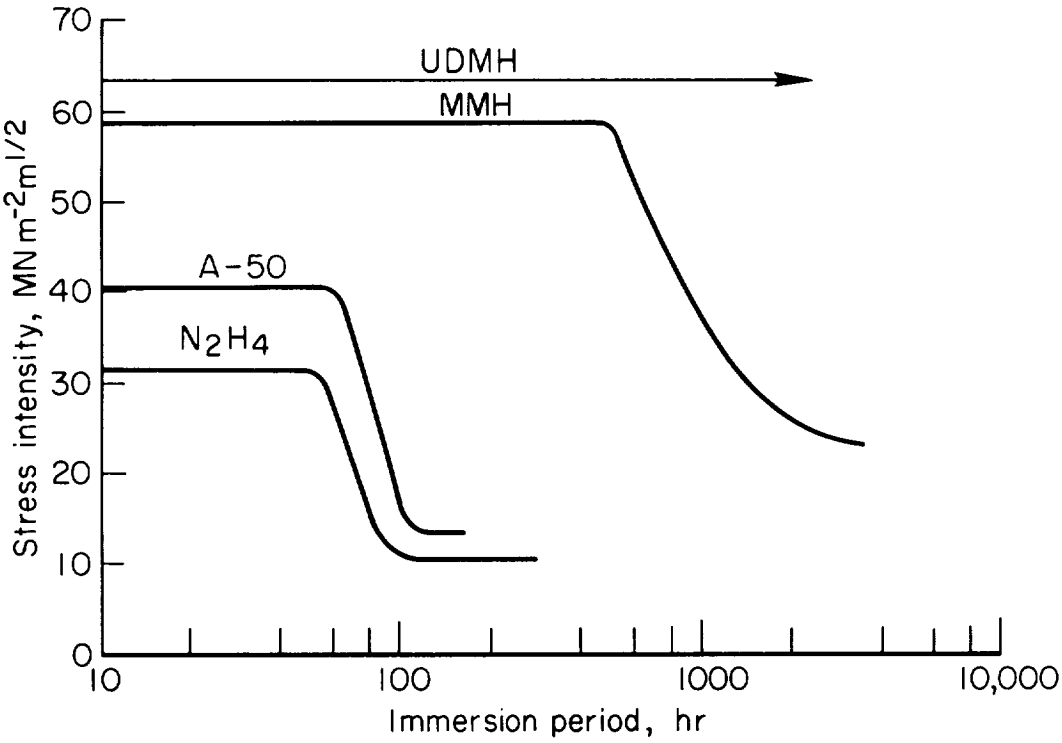

Figure 5.– The stress corrosion of 4130 steel in four propellants.

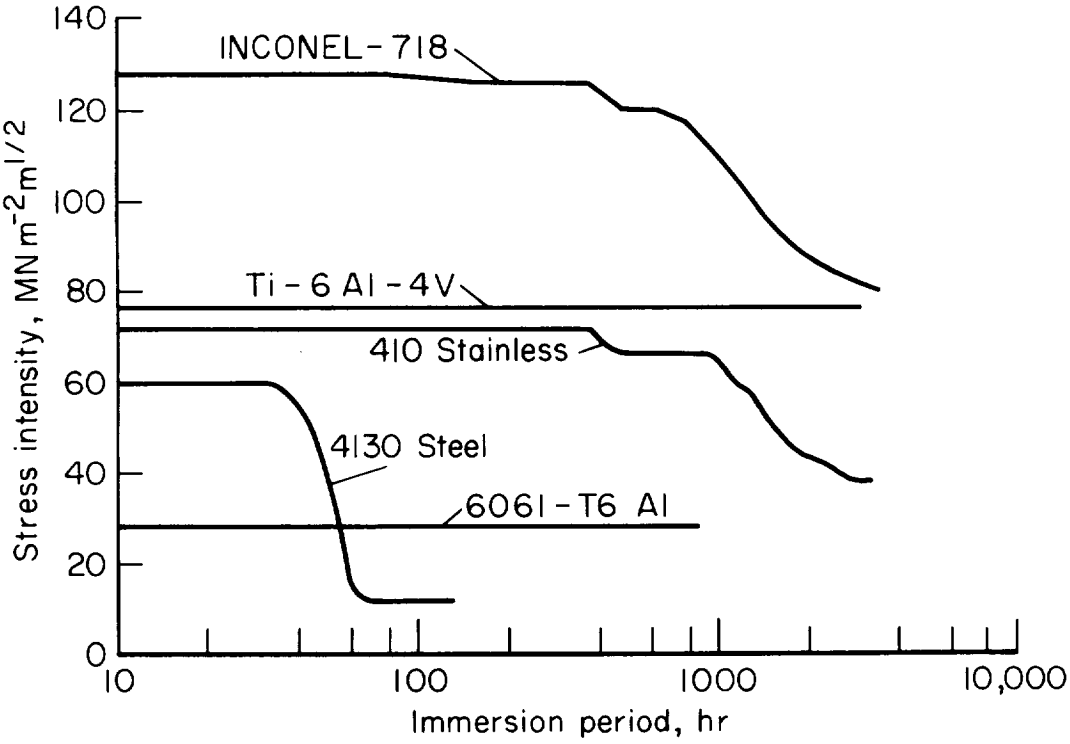

Figure 6.– The stress corrosion susceptibility of several alloys in hydrazine.

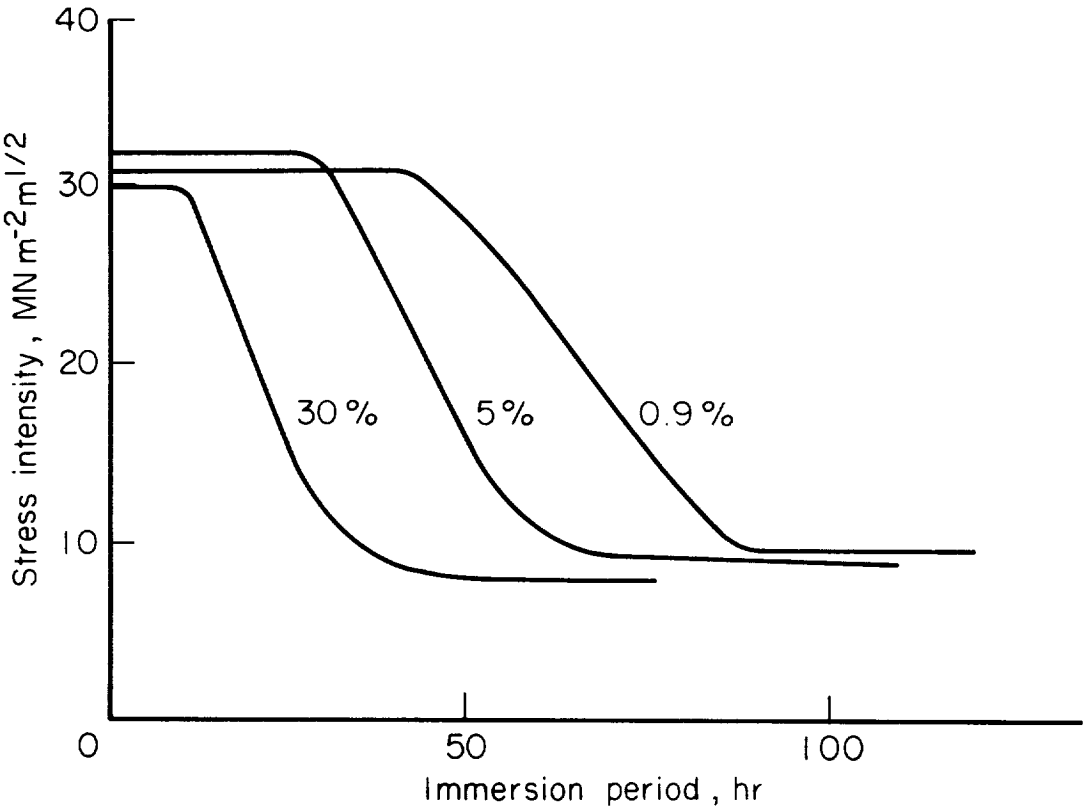

Figure 7.– The effect of water content in hydrazine on the stress corrosion susceptibility of 4130 steel.

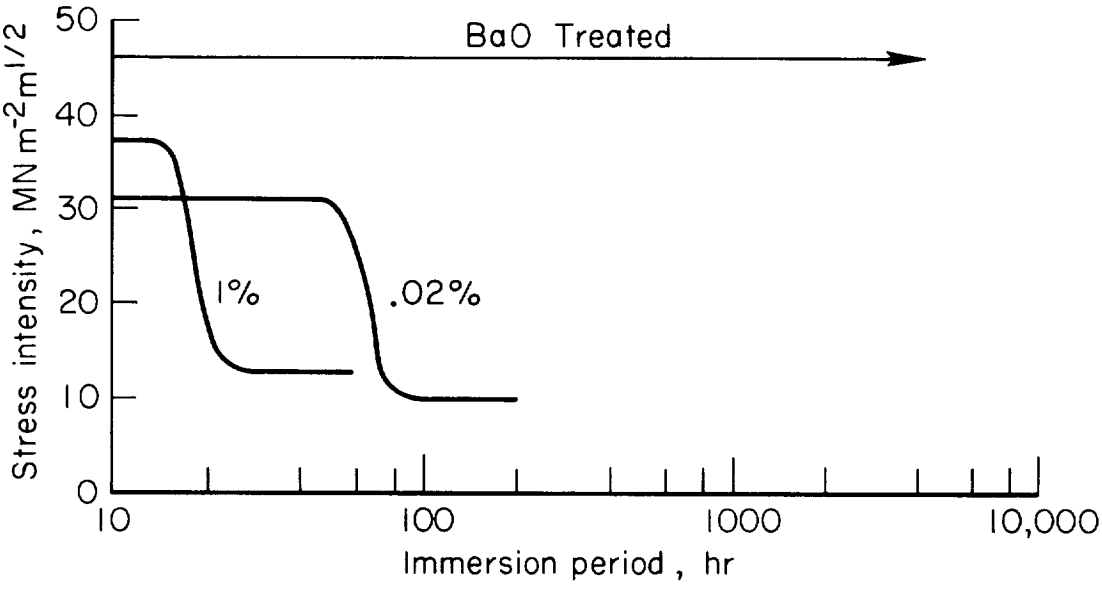

Figure 8.– The effect of carbon dioxide level in hydrazine on the stress corrosion susceptibility of 4130 steel. (Effective CO_2 level in BaO treated hydrazine probably <0.005 percent.)

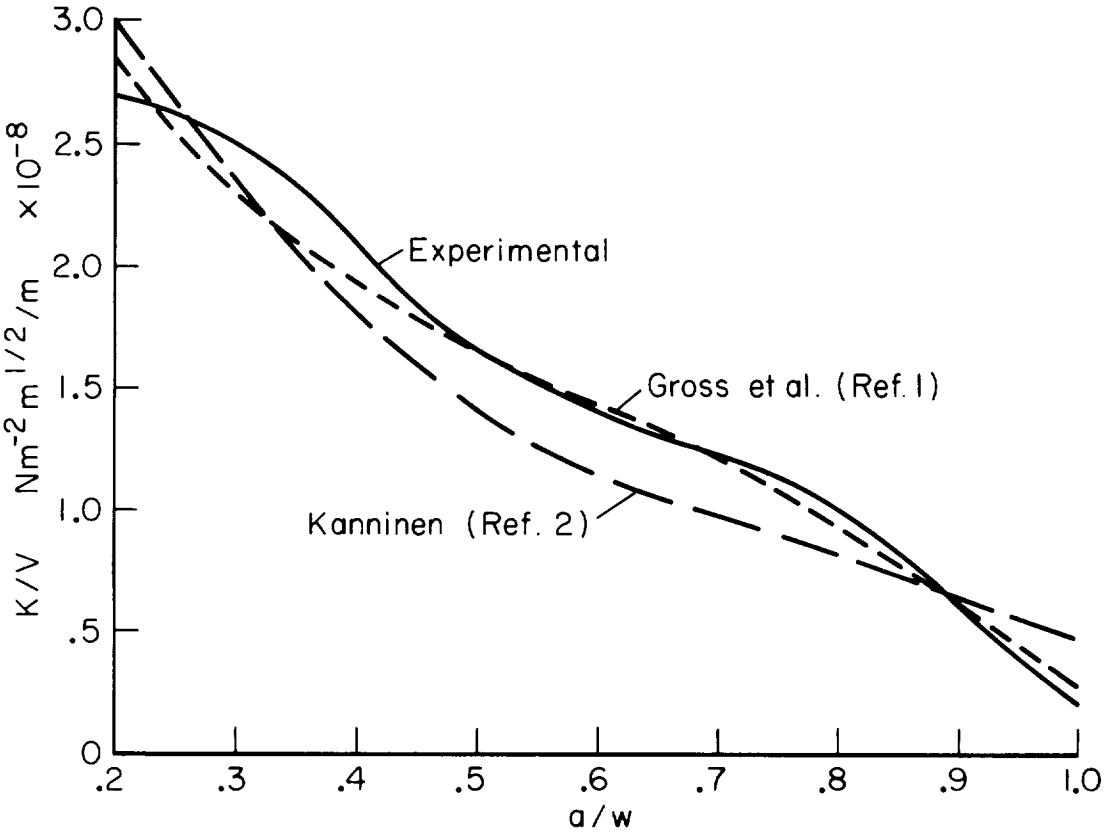

Figure 9.– Test specimens stress intensity response at a given crack mouth displacement as a function of crack length.